Computer modeling of RF ablation in cortical osteoid osteoma:

Assessment of *insulating* effect of the reactive zone

Ramiro M Irastorza[1,2], Macarena Trujillo[3], Jose Martel Villagrán[4], Enrique Berjano[5]

[1] *Instituto de Física de Líquidos y Sistemas Biológicos (CONICET), La Plata, Argentina*

[2] *Instituto de Ingeniería y Agronomía, Universidad Nacional Arturo Jauretche, Argentina*

[3] *Instituto Universitario de Matemática Pura y Aplicada, Universitat Politècnica de València, Spain*

[4] *Radiodiagnostic Department, Hospital Universitario Fundación Alcorcón, Madrid, Spain*

[5] *Biomedical Synergy, Electronic Engineering Department, Universitat Politècnica de València, Valencia, Spain*

Corresponding author: Dr. Ramiro M Irastorza, Instituto de Física de Líquidos y Sistemas Biológicos (CONICET), Calle 59 No 789, B1900BTE La Plata, Argentina Phone: +54-221-4233283, Fax:+54-221-4257317, E-mail: rirastorza@iflysib.unlp.edu.ar

1

Abstract

Purpose: To study by computer simulations the insulating role of the reactive zone surrounding a cortical osteoid osteoma (OO) in terms of electrical and thermal performance during radiofrequency ablation (RFA).

Material and methods: We modeled a cortical OO consisting of a nidus (10 mm diameter) enclosed by a reactive zone. The OO is near a layer of cortical bone 1.5 mm thick. Trabecular bone partially surrounds the OO and there is muscle around the cortical bone layer. We modeled RF ablations with a non-cooled-tip 17G needle electrode (300 s duration and 90ºC target temperature). Sensitivity analyses were conducted assuming a reactive zone electrical conductivity value (σ_{rz}) within the limits of the cortical and trabecular bone, i.e. 0.02 S/m and 0.087 S/m, respectively. In this way we were really modeling the different degrees of osteosclerosis associated with the reactive zone.

Results: The presence of the reactive zone drastically reduces the maximum temperature reached outside it. The temperature drop is proportional to the thickness of the reactive zone: from 68ºC when it is absent to 44ºC when it is 7.5 mm thick. Higher nidus conductivity values (σ_n) implied higher temperatures, while lower temperatures meant higher σ_{rz} values. Changing σ_{rz} from 0.02 S/m to 0.087 S/m reduced lesion diameters from 2.4 cm to 1.8 cm.

Conclusions: The computer results suggest that the reactive zone plays the role of insulator in terms of reducing the temperature in the surrounding area.

Keywords: Computer modeling, cortical bone, finite element method, osteoid osteoma, radiofrequency ablation, reactive zone.

1. Introduction

Osteoid osteoma (OO) is a common bone tumor, representing approximately 10% of all benign skeletal lesions, that involves progressively worsening pain [1]. Although OO is benign and spontaneous remission occasionally occurs, an intervention for definitive relief of pain is sometimes required [2]. Among others techniques [3], radiofrequency ablation (RFA) is a minimally invasive technique which allows thermal destruction of the OO [4-6]. The most common location of OO is in the long bones [5]. Most OOs are cortical and macroscopically consist of a nidus of active bone surrounded by a reactive zone. The nidus, usually 5–10 mm in diameter [2], is the actual tumor, and hence the target of the RFA. The reactive zone of a cortical OO is partially surrounded by the cortex (cortical bone) while the rest is enclosed by trabecular bone (Figure 1). It has been suggested that the presence of cortical bone during RFA could play the role of a thermal insulator and hence grant protection to the adjacent soft tissues [7-9]. We have already observed this performance in a previous modeling study [10], which could be explained by the lower electrical conductivity of the cortical bone than the surrounding tissues.

The reactive zone is histologically characterized by very dense reactive sclerotic bone [1] and can in fact be radiographically observed as a cortical thickening. For these reasons, and even though there are no experimental data available on electrical and thermal characteristics of the reactive zone, one could assume that its characteristics could somehow be similar to those of cortical bone. With all these issues in mind, we hypothesized that the reactive zone could also play an important role as thermal insulation during RFA of a cortical OO. As a detailed assessment of this issue has not been carried out to date, our aim was to build computer models to study the temperature distributions during RFA in the tissues involved in a cortical OO, with a special focus

3

on assessing the possible *insulating* effect of the reactive zone and identifying the factors involved. Computer modeling technique is a methodological approach broadly employed to study the impact of factors on temperature distributions during RF heating of biological tissues [11].

2. Materials and methods

2.1. Physical situation

We considered a spherical nidus surrounded by a reactive zone, more or less next to the cortex of a long bone. Access to the OO to conduct an ablation is not a straightforward task. Firstly, a biopsy trochar is advanced under image guidance to the cortex (cortical layer). Then, the cortex is drilled to within 1 mm or less of the tumor [6]. The RF applicator, which includes a metallic electrode on its distal part, is introduced into the nidus through the drill hole [12] (Figure 1a). The result of this approach is a physical arrangement as sketched in Figure 1b, in which the RF applicator passes through the cortical bone, and is exactly the physical situation modeled in this study. We considered a non-cooled tip needle-like electrode with 17G diameter and a 5 mm exposed tip (including a sharp zone 1 mm long).
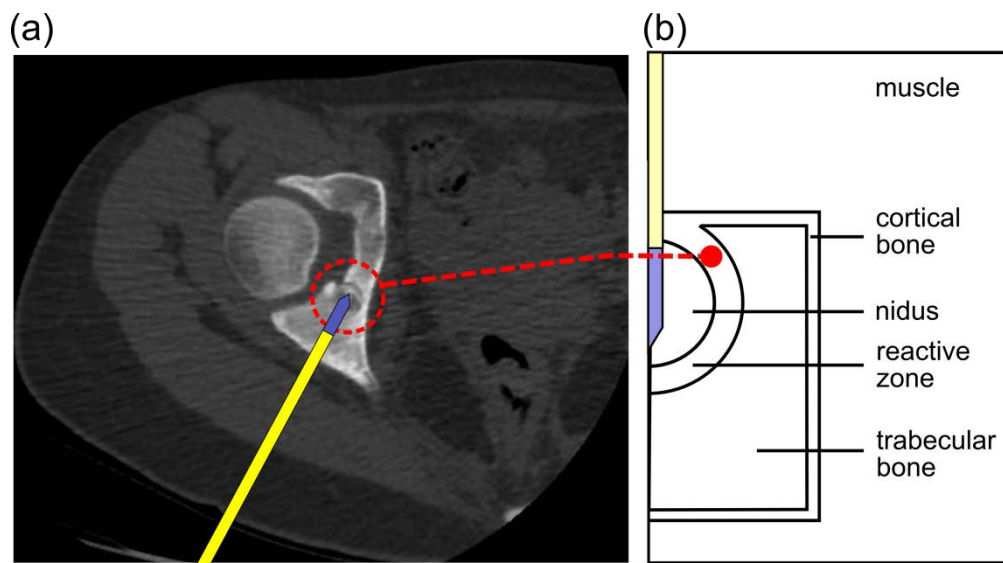
Figure 1 (a): Cortical osteoid osteoma consisting of a nidus surrounded by cortical and trabecular bone. The RF applicator is introduced into the nidus through a drill hole prior to RF application. (b): Theoretical model of cortical OO consisting of a nidus enclosed by a reactive zone.

2.2. Geometry of the model

Figure 1b shows the geometry of the cortical OO model, consisting of a nidus (10 mm diameter) enclosed by a reactive zone of variable thickness (2.5, 5.0 and 7.5 mm). We considered two relative positions of the OO and the cortical bone layer, as shown in Figure 2 (Positions 1 and 2). Both positions are relevant because they represent the two limits between which the cortical OO can be located in relation to the cortical bone layer, which was assumed to be 1.5 mm thick. Position 2 represents a case in which the presence of the OO has caused a periosteal reaction, i.e. an elevation of the periosteum from the cortex [13]. The model includes muscle beyond this layer. Likewise, we defined three relevant directions in which temperature profiles were computed: -45º, 0º and 45º (all with the origin at the midpoint of the electrode surface). In this way three points (T_{45}, T_0 and T_{-45}) were defined to assess the temperature beyond the reactive zone and composed the intersection points between these directions and the outer layer of the reactive zone.

Position 1   Position 2

5
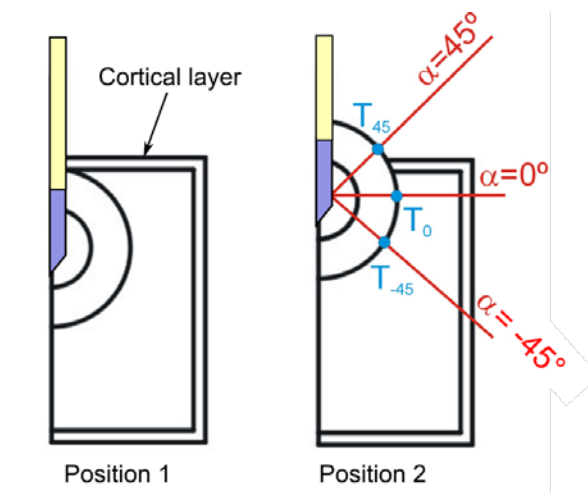
Figure 2 Relative positions of the OO and the cortical bone layer. We defined three

directions in which temperature profiles were computed: -45º, 0º and 45º

(origin at the midpoint of the electrode surface). Note that in Position 2, the

45º direction, has muscle tissue outside the reactive zone, while 0º and -45º

have trabecular muscle. The intersection points between these directions and

the outer layer of the reactive zone defined three locations at which the

temperature was assessed (T_{45}, T_0 and T_{-45}).

2.3. Governing equations, numerical method and boundary conditions

The model was based on a coupled electric-thermal problem in which the governing

equation for the thermal problem was the bioheat equation, which was modified by the

enthalpy method to take into account the vaporization phenomenon in the tissues [14]:

$$\frac{\partial(\rho h)}{\partial t} = \nabla \cdot (k \nabla T) + q_{RF} + Q_p + Q_{met} \tag{1}$$

where ρ is tissue density, h enthalpy, k thermal conductivity, T temperature and t time.

q_{RF} refers to the heat source from RF power, Q_p refers to the blood perfusion heat and

Q_{met} refers to the metabolic heat, which is negligible in RFA. For biological tissues

enthalpy is related to tissue temperature by the following expression [14]:

$$\frac{\partial(\rho h)}{\partial t} = \frac{\partial T}{\partial t} \cdot \begin{cases} \rho_l c_l & 0 < T \leq 99°\,C \\ h_{fg} C & 99 < T \leq 100°\,C \\ \rho_g c_g & T > 100°\,C \end{cases} \tag{2}$$

where ρ_i and c_i are density and specific heat of tissue respectively at temperatures below

100ºC ($i=l$) and at temperatures above 100ºC ($i=g$), h_{fg} is the product of water latent

heat of vaporization and water density at 100ºC, and C is tissue water content inside the

tissue. The blood perfusion heat Q_p is computed from:

$$Q_p = \beta \rho_b c_b \omega_i (T_b - T) \tag{3}$$

where ρ_b is density of blood, c_b specific heat of blood, T_b blood temperature (37ºC), ω_i perfusion coefficient of the tissue i, and β is a coefficient which took the values of 0 and 1, according to the value of the temperature reached: $\beta = 0$ for T $\geq$ 50ºC, and $\beta = 1$ for T $<$ 50ºC. Although some models included a slight increase in blood perfusion flow with initial temperature elevation [15], it has been demonstrated that the most important effect is the ceasing/decreasing due to the thermal coagulation.

The heat source q_{RF} is the distributed heat source due to the Joule effect (loss) which is given by:

$$q_{RF} = \sigma|\boldsymbol{E}|^2 \tag{4}$$

where σ (S/m) is electrical conductivity at 500 kHz, and $|\boldsymbol{E}|$ the magnitude of the vector electric field (V/m), which is given by $\boldsymbol{E} = -\nabla V$. The Laplace equation governs the conductive media, and allows voltage V to be calculated:

$$\nabla \cdot \sigma \nabla V = 0 \tag{5}$$

At RF frequencies ($\approx$500 kHz) and over the distance of interest, the biological medium can be considered almost totally resistive and a quasi-static approach is therefore possible to solve the electrical problem [16].

The coupled electrical-thermal problem was numerically solved using COMSOL Multiphysics (Comsol, Burlington, MA, USA). We performed convergence tests to determine the adequate size of domain limits, and spatial and temporal resolution. Spatial resolution was achieved by refining the mesh so that the maximum temperature reached in the tissue after 300 s (T_{max}) was within 0.5% of the value obtained from the previous refinement step. When an adequate spatial resolution was achieved, we decreased the time step until T_{max} was within 0.5% of the value obtained from the previous time step.

There are several protocols for delivering electrical power in RFA of OO. In general, a constant temperature mode is clinically used with a target temperature of 90ºC and duration ranging from 240 s [4,17-19] to 360 s [20]. We considered this same mode with a target temperature of 90°C and duration of 300 s. To implement the constant temperature mode we used the same approach as in [21], in which the authors considered a dynamic system for control purposes. The input variable of the system was the voltage applied to the electrode (V_e) and the output variable was the temperature measured at the tip of the electrode (T_e). There are different ways of controlling tip temperature, such as PID, adaptive, neural network prediction and fuzzy logic control [21]. We considered a proportional-integral (PI), which is defined by the parameters K_p and K_i, with values of 1.15 and 0.06, respectively.

Electrical boundary conditions were: zero current density at the axis, zero voltage at the lower limit (to mimic the dispersive electrode) and voltage at the active electrode. Initial temperature and the temperature for the surfaces away from the active electrode were assumed to be 37ºC.

2.4. Physical characteristics of the model

Table 1 shows the values of the physical characteristics of the materials used in the model [22,23]. The thermal conductivity and specific heat of cortical bone and muscle were taken from a previous sensitivity analysis [10]. A change in σ with temperature was considered of +1.5 %/°C (with an abrupt drop when temperature reaches 100°C) and also a change in k with temperature of +0.003 K^{-1} (with a constant value above 100ºC) for the tissues [24]. The internal tissue water content (C in Eq. 2) was assumed to be 68% [25].

As far as we can ascertain, there are no data available on the electrical and thermal characteristics of the nidus and the reactive zone. Most of the physical data on tumor tissue is taken from human and animal models of breast carcinoma [26-28]. In this study, electrical conductivity (σ) of both tissues was considered to be within reasonable ranges, and computer simulations were conducted to assess the sensitivity of each parameter. To be more precise, since the nidus is composed of vascularized connective tissue [29], we assumed that its electric conductivity (σ_n) would not be very different from that measured in human breast carcinoma (within 0.08 S/m and 0.5 S/m, see [28]). We considered σ_n values of 0.08, 0.22, 0.36 and 0.50 S/m.

The reactive zone corresponds histologically with a very dense reactive sclerotic bone [1], so that we can assume a value of σ_{rz} within these limits coinciding with the σ of cortical and trabecular bone, i.e. 0.02 S/m and 0.087 S/m, respectively. In this way we are really modeling the different degrees of osteosclerosis associated with the reactive zone. We considered 0.02, 0.042, 0.065 and 0.087 S/m as σ_{rz} values. The thermal characteristics of the reactive zone were assumed to be identical to those of cortical bone. Rossmanna and Haemmerich [26] reviewed the thermal properties of adenocarcinoma in the human breast and we took these values for the specific heat and the thermal conductivity of the nidus.

The indicator for heat-sink strength by blood perfusion is the blood perfusion rate (m), usually expressed in mL/min/100 g [30]. In order to consider this parameter in Eq. (3), the perfusion coefficient (ω_i) must be computed. The perfusion coefficient of the tissue i is related to m_i as follows: $\omega_i = m_i \rho_i 10^{-5}/60$. For instance, the mean value for trabecular bone in humans is $m = 1$ mL/min/100g [30] which corresponds to a ω_i value of approximately 1.967×10^{-4} s^{-1}. In [30], authors reported a perfusion coefficient of zero for cortical bone, while in [22] a mean value of 3.18×10^{-4} s^{-1} was reported. Due to the

lack of data on perfusion in the reactive zone, and in accordance with the histological criterion mentioned above, we assumed a range of values of ω_i within these limits, coinciding with cortical and trabecular bone, i.e. 1.967×10^{-4}, 3.933×10^{-4} and $5.9\times10^{-4}\text{s}^{-1}$ (see Table 1). In contrast, since the nidus is a well vascularized tissue [29] we assumed values between 26×10^{-4} s^{-1} and 70×10^{-4} s^{-1}, which are the minimum and maximum values measured by [31]. The following values were thus considered: 26×10^{-4}, 41×10^{-4}, 55×10^{-4} and 70×10^{-4} s^{-1}.

Table 1. Physical properties of the materials used in the model.

Material/Tissue	Density (kg/m³)	Electrical conductivity (S/m)	Thermal parameters (@37ºC)		
			Specific heat (J/kg K)	Thermal conductivity (W/m K)	Blood perfusion coefficient ($\times10^{-4}\text{s}^{-1}$)
Cortical bone	1908	0.022	1026 [a]	0.30 [a]	0 [c]
Trabecular bone	1178	0.087 [b]	2274	0.31	5.9
Nidus	1046	0.08 [d] – 0.5 [d]	2726 [e]	0.56 [e]	26 [f] – 70 [f]
Reactive zone	1908	0.02 – 0.087	1026	0.30	0 [c] – 5.9
Muscle	1090	0.446	2824 [a]	0.52 [a]	6.7
Blood	1046	-	3639	-	-
Plastic (insulated trocar)	70	10^{-5}	1045	0.026	0
Electrode	6450	10^{8}	840	18	0

All tissue data from [22] except: [a][10], [b][32], [c][30], [d][28], [e][26], [f][31]. Data for insulated trocar (plastic) and electrode from [23].

2.5. Outcomes

The only target of the RFA is the nidus and not the surrounding tissue. The situation is not critical if the adjacent tissue is reactive bone. On the other hand, when there is not a sufficient degree of sclerosis soft tissues such as vessels and nerves can suffer thermal

injury. For this reason, and also to broadly assess the insulating role of the reactive zone, we studied the maximum temperature reached at the outer boundary of the reactive zone, and in particular, in two very dissimilar areas: muscle (45º direction, see Figure 2) and trabecular bone (directions 0º and -45º, see Figure 2). We also studied other variables involved in RFA, such as impedance and the distributed heat source (q_{RF}), which could provide a physical explanation of the computer results. The 50ºC isotherm was used to represent the thermal lesion contour.

3. Results

The appropriate size of the model domains limits was a width of 21.5 mm and a height of 33 mm. The models had around 8,000 triangular elements and a time step of 0.01 s was used for each simulation.

3.1. Effect of perfusion coefficient and electrical conductivity

In the first set of simulations we considered an OO in Position 2 with a reactive zone 5 mm thick. We analyzed the maximum temperatures reached at the outer boundary of the reactive zone, in particular at the interface with the trabecular bone (T_0) and muscle (T_{45}). In these simulations a sensitivity analysis was conducted by simultaneously varying the electrical conductivity and perfusion coefficient of the nidus and reactive zone. As shown in Figure 3, temperatures at the reactive zone-trabecular bone (T_0) were slightly higher (around 1–2ºC) than at the interface reactive zone-muscle (T_{45}). Overall, the perfusion coefficients of nidus and reactive zone did not appear to have an influence on the temperatures reached at the outer limit of the reactive zone (Figure 3a and b).

In contrast, the effect of σ_n and σ_{rz} was important, and surprisingly, was the opposite in each, i.e. while an increase in σ_n involved an increase in both T_0 and T_{45}, an increase

in σ_{rz} involved a decrease. Both T_0 and T_{45} varied by around 5ºC when σ_n and σ_{rz} were varied. Once more, temperatures at the outer layer of the reactive zone on the trabecular bone side (T_0) were 1–2ºC higher than on the muscle side (T_{45}).
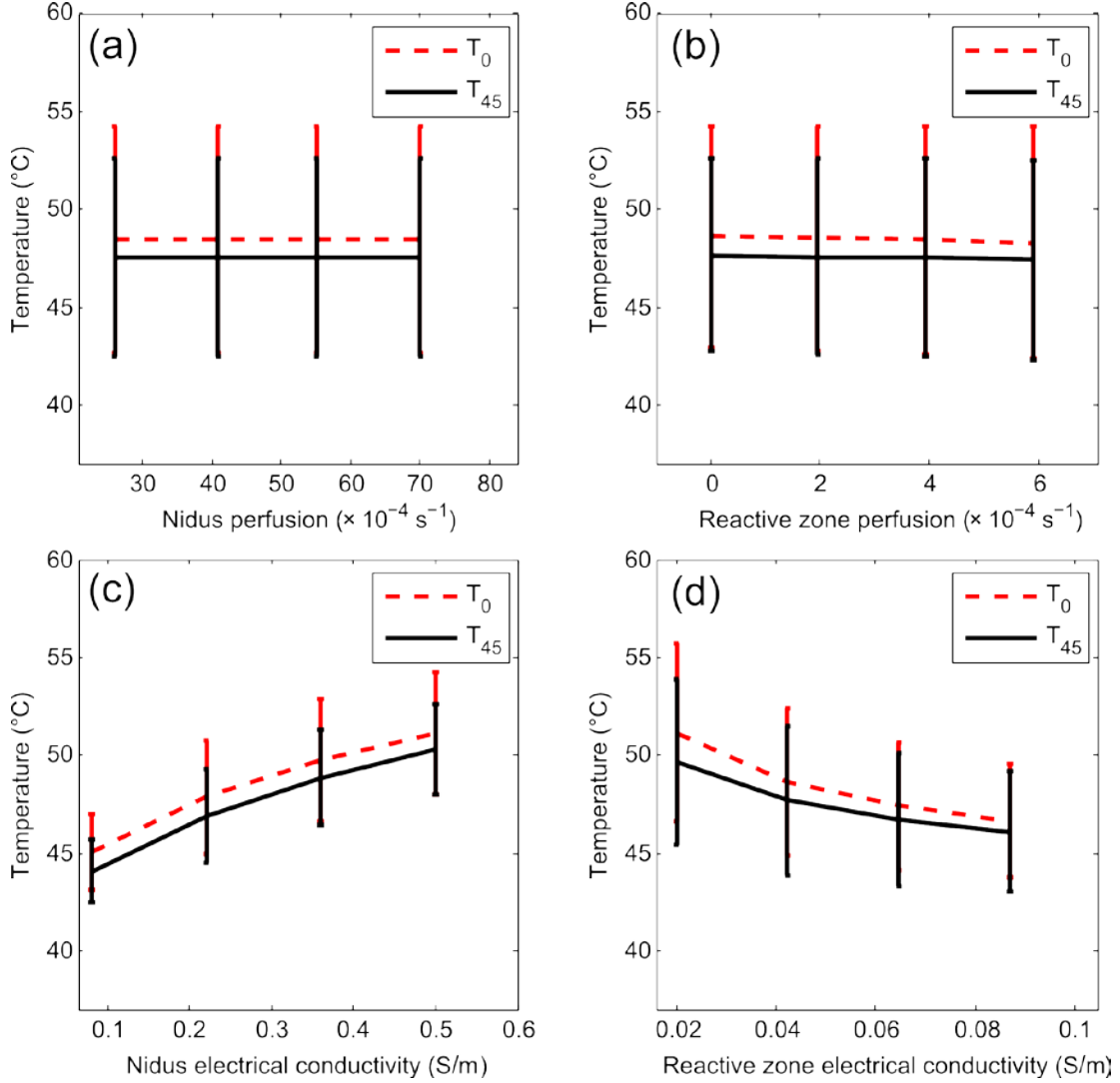

Figure 3   Maximum temperatures reached after 300 s of RFA at the outer limit of the reactive zone, in particular in the interface with trabecular bone (T_0) and with muscle (T_{45}) for different values of perfusion coefficient of nidus (ω_n) and reactive zone (ω_{rz}) (a and b), and of electrical conductivity of nidus (σ_n) and reactive zone (σ_{rz}) (c and d). 64 simulations were conducted for each specific value of one of these parameters, varying the other three parameters (four values within a range). We then calculated and plotted the mean value of the 64 simulations. The maximum value of the difference with respect to the mean value was also plotted

as a dispersion bar. These simulations were conducted with the OO in Position 2 (see Figure 2).

In order to check that the behavior shown in Figure 3(c and d) is not due to the entire parameter being changed simultaneously, in Figure 4 we plotted the change of temperature profile along the 0° direction with the change in σ_{rz} (keeping σ_n constant with a mean value of 0.29 S/m) and with the change in σ_n (for a mean value of σ_{rz} of 0.0535 S/m). Figure 4 confirms that for higher values of σ_n, temperatures at the end of the RFA are higher. In contrast temperatures at the end of the RFA are lower for higher values of σ_{rz}. In terms of thermal lesion, a change in σ_{rz} from 0.02 S/m (reactive zone with high degree of osteosclerosis) to 0.087 S/m (reactive zone with characteristics very similar to trabecular bone) reduces lesion diameter from 24 mm to 18 mm. Although the effect of changing σ_n is the opposite, it is more or less similar in absolute values of change in the lesion diameter.

Figure 4 also shows that in general the temperature drop with distance inside the reactive zone is steeper than in the nidus zone, which suggests that the presence of the reactive zone somehow limits the lesion volume (this issue is analyzed below).
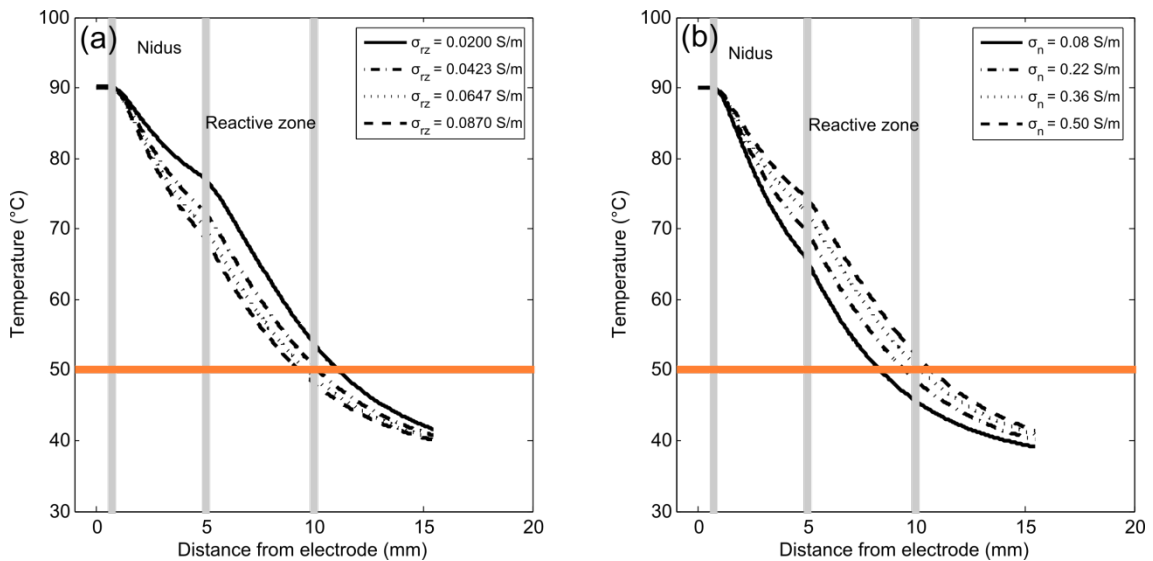
Figure 4   Temperature profiles (at 300 s) computed in the 0º direction (see Figure 2) for different electrical conductivity values of the reactive zone (a) and nidus (b). The 50ºC line represents the thermal lesion contour. These simulations were conducted with the OO in Position 2 (see Figure 2).

To determine the reasons for the different behavior of the nidus and reactive zone in terms of electrical conductivity, we analyzed the spatial distribution of the resistive heating q_{RF} at end of ablation (300 s). Figure 5 shows q_{RF} distribution of the tissues involved for different values of σ_n and σ_{rz}. As can be expected, q_{RF} drops drastically around the electrode. The differences of q_{RF} in the nidus when σ_n and σ_{rz} vary do not seem to be relevant; however there are interesting differences in the reactive zone. The differences shown in Figure 5a are in agreement with the temperature profiles seen in Figure 4a: An increase in σ_{rz} implies a decrease in q_{RF} (and consequently in temperature). The differences in Figure 5b are rather more subtle and cannot be explained so easily.
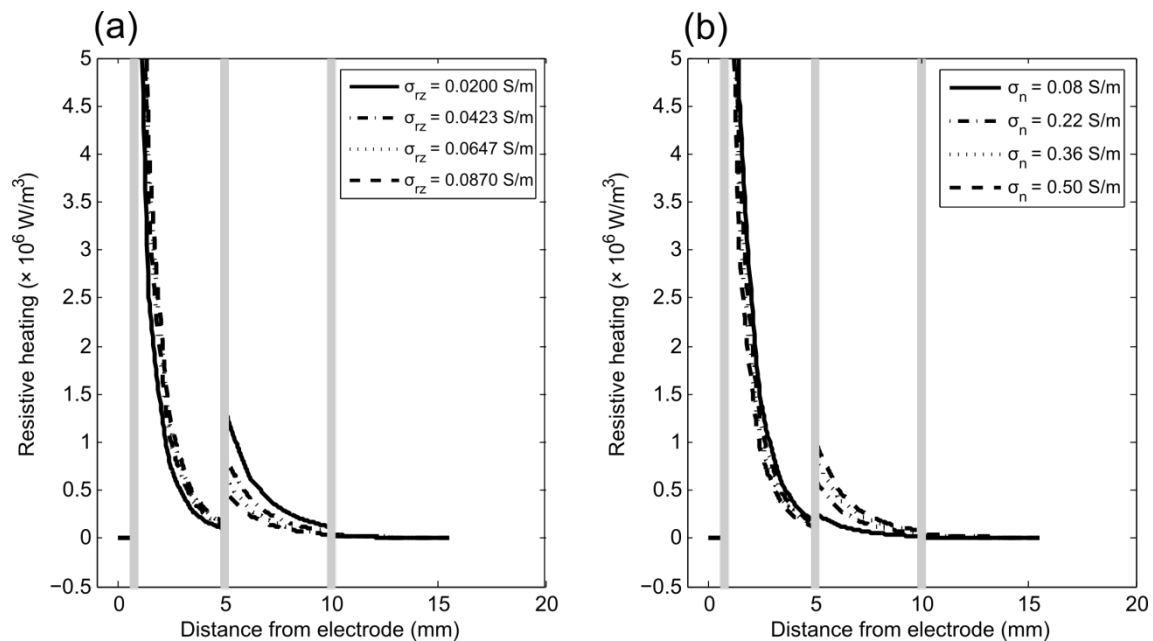
Figure 5   Distributed heat source q_{RF} due to RF power in the involved tissues for different

values of electrical conductivity of reactive zone σ_{rz} (a) and nidus σ_n (b). These

simulations were conducted with the OO in Position 2 (see Figure 2).

Figure 6 shows the progress of the applied voltage throughout RFA for different

values of σ_n and σ_{rz}. Note that the change of σ_{rz} causes larger changes in the applied

voltage than changes of σ_n. In general, an increase in the electrical conductivity implied

a decrease in the applied voltage.
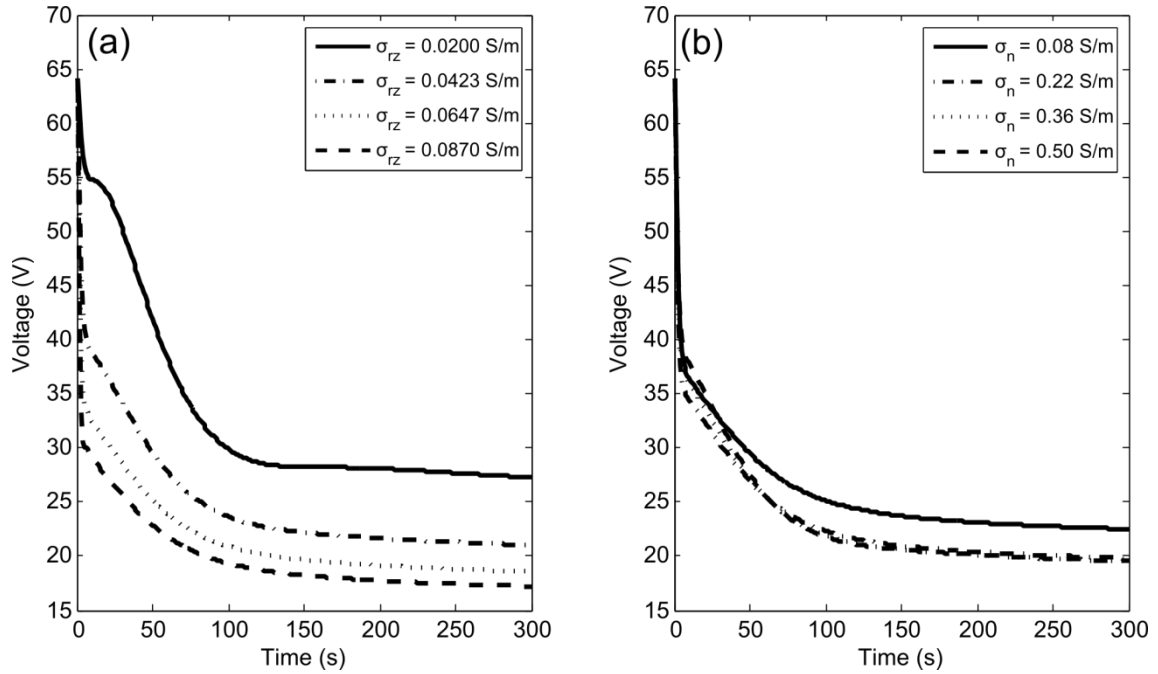
Figure 6   Progress of the applied voltage throughout RF ablation for different values of

electrical conductivity of the reactive zone σ_{rz} (a) and nidus σ_n (b). These

simulations were conducted with the OO in Position 2 (see Figure 2).

3.2. Effect of reactive zone (RZ) thickness

Figure 7 shows the temperature distributions at the end of RFA and the thermal lesion

contour evolution for different RZ thicknesses. These simulations were conducted with

OO in Position 1 (see Figure 2). The results show that RZ thickness has little effect on

the temperature distributions across the mathematical domain, regardless of tissue type. Obviously, the thinner the reactive zone, the faster the thermal lesion contour reaches the area beyond it. Also, the thermal lesion enlarges almost homogeneously, i.e. growth is identical regardless of direction (α).
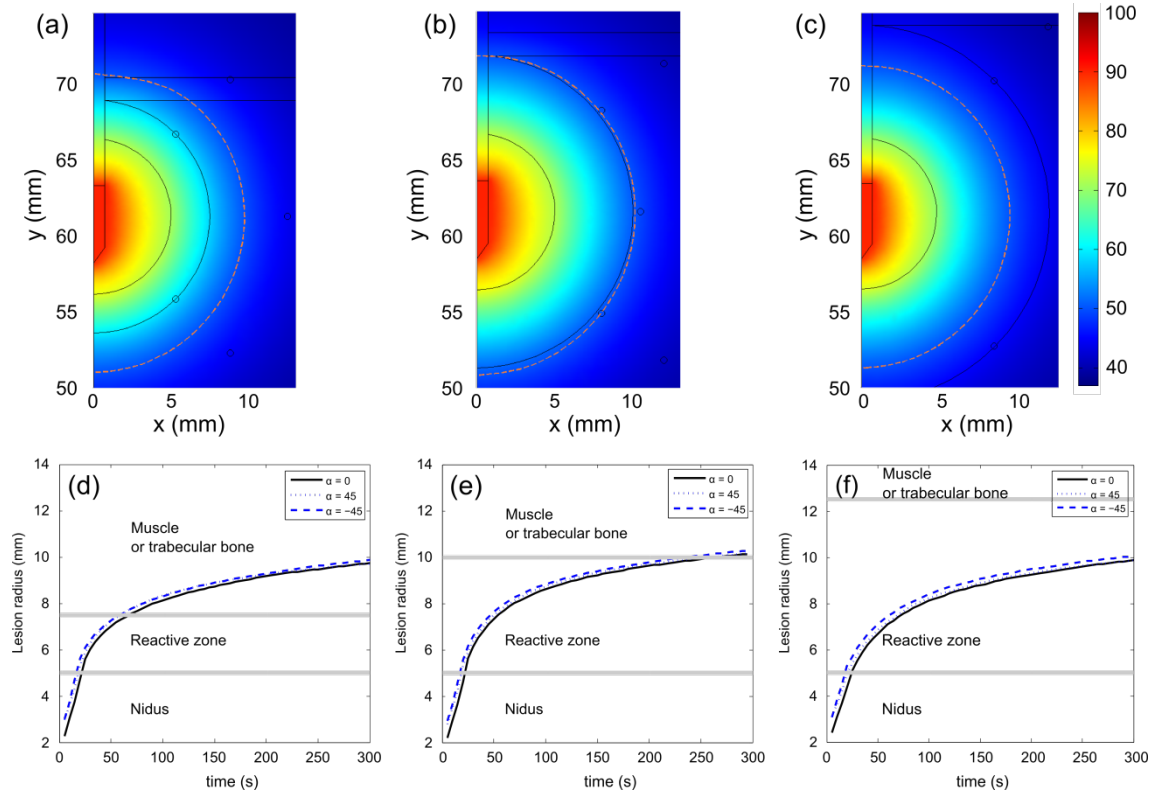
Figure 7   Temperature distributions (in ºC) after 300 s of RFA for three RZ thicknesses: 2.5 mm (a), 5.0 mm (b) and 7.5 mm (c). Dashed line is the 50ºC isoline which represents thermal lesion contour. Progress of the thermal lesion radius throughout 300 s of RFA at the outer limit of the reactive zone for three RZ thicknesses: 2.5 mm (d), 5.0 mm (e) and 7.5 mm (f), and for three directions ($\alpha=0$, 45º and -45º). These simulations were conducted with the OO in Position 1 (see Figure 2).

Table 2 and Figure 8 show the electrical impedance (Ω) recorded at the start of RFA for different RZ thicknesses and electrical conductivity (σ_{rz}). Note that the effect of RZ

thickness is especially important when σ_{rz} is very low, which is found when there is a high degree of osteosclerosis (reactive zone with characteristics similar to cortical bone). For medium and high σ_{rz} values, the thickness has very little effect on impedance. Table 3 shows the electrical impedance for different RZ thickness and electrical conductivity in the nidus (σ_n).

Table 2. Electrical impedance (Ω) at the start of RFA for different RZ thickness and electrical conductivity (σ_{rz}).

		Thickness (mm)					
		2.5		5.0		7.5	
		Position 1	Position 2	Position 1	Position 2	Position 1	Position 2
	0.02	511.1	490.3	616.8	598.1	680.1	694.1
	0.042	363.4	338.2	400.1	377.4	422.2	427.7
σ_{rz} (S/m)	0.065	314.6	285.4	328.6	302.5	337.4	328.2
	0.087	289.7	257.2	291.6	262.8	293.3	287.1

Table 3. Electrical impedance (Ω) at the start of RFA for different RZ thickness and electrical conductivity of the nidus (σ_n).

		Thickness (mm)					
		2.5		5.0		7.5	
		Position 1	Position 2	Position 1	Position 2	Position 1	Position 2
	0.08	703.3	677.2	727.3	697.6	742.0	773.6
	0.22	376.6	348.9	400.3	374.7	414.8	421.2
σ_n (S/m)	0.36	308.6	281.7	331.4	307.7	345.4	346.3
	0.50	279.0	252.8	301.2	278.5	314.8	310.9
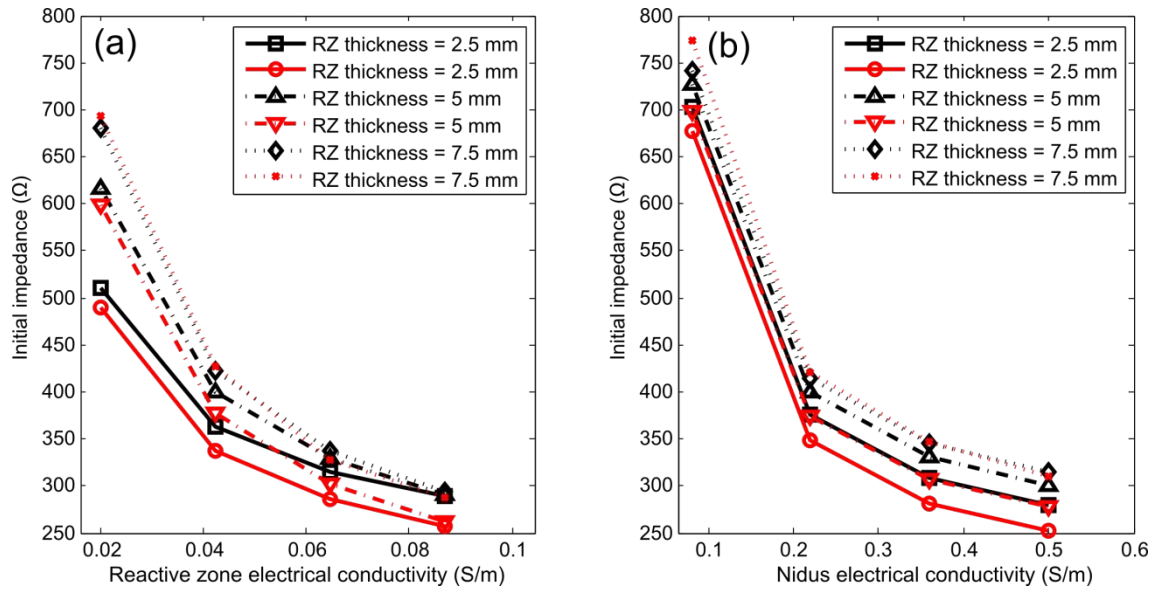
Figure 8   Effect of electrical conductivity of nidus (σ_n) and reactive zone (σ_{rz}) on electrical impedance (Ω) registered at start of RFA. The effect of RZ thickness and OO position are also considered. Black and red colors correspond with Position 1 and 2, respectively. Trend lines have been added as a guide.

3.3. Effect of presence of the reactive zone

Although a marked reactive sclerosis is commonly found around the nidus, some lesions may have little or no reactive sclerosis [33], which led us to conduct computer simulations without a reactive zone, considering the mean values of σ_n and σ_{rz} (0.29 and 0.0535 S/m, respectively). Figure 9 shows the temperature profiles at the end of RFA for different RZ thicknesses and with no RZ. In the latter case, since we were modeling Position 1, the nidus is in direct contact with the trabecular bone. Note that the case with no RZ in Position 2 is fictitious, since a bone layer has to necessarily surround the nidus.
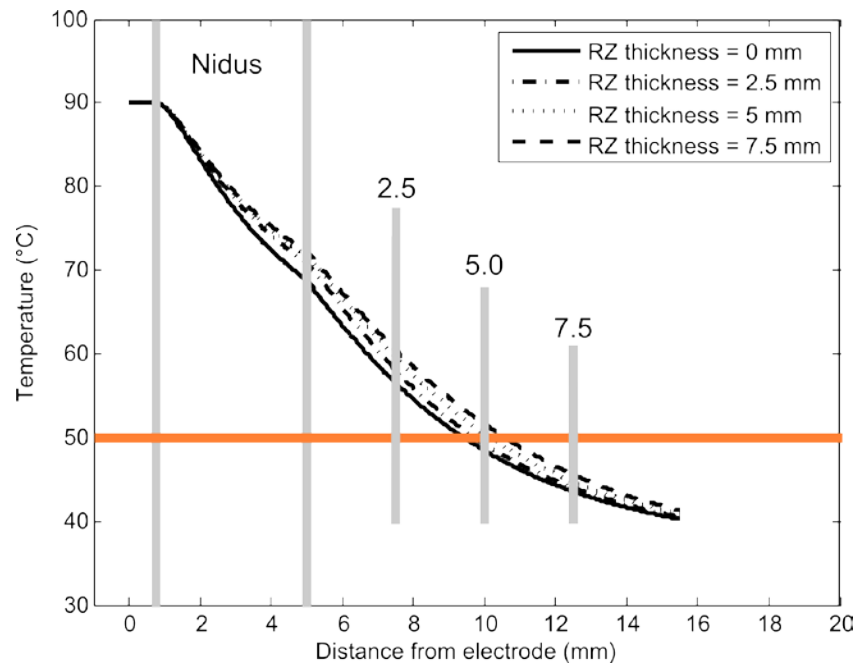
Figure 9   Temperature profiles (at 300 s) computed in 0º direction (see Figure 2) for different RZ thicknesses. The case without a reactive zone is also plotted (solid line). The 50ºC line represents the thermal lesion contour. All simulations were conducted with OO in Position 1 (see Figure 2).

Figure 9 suggests that the presence of a reactive zone drastically reduces the maximum temperature reached in the trabecular bone. The drop in the maximum temperature is proportional to RZ thickness: from 68ºC when it is absent to 44ºC at a thickness of 7.5 mm. However, surprisingly, the presence of a reactive zone around the nidus involves an augment in the temperature profiles (see Fig. 9). This difference may be up to ≈5ºC between the absence of an RZ and a thickness of 7.5mm. From this it would seem that the reactive zone does not itself provide an insulating effect.

Initial impedance in the absence of a reactive zone was ≈ 45 Ω lower than an RZ thickness of 2.5 mm: 656.8 Ω, 330.7 Ω, 265.2 Ω, and 237.1 Ω, for σ_n of 0.08, 0.22, 0.36 and 0.5 S/m, respectively.

Discussion

We conducted computer simulations aimed at assessing the electrical and thermal performance of the reactive zone during RFA of a cortical OO. In this assessment we assumed that the electrical conductivity of the reactive zone depends on the degree of osteosclerosis of the RZ: from 0.02 S/m for severe osteosclerosis to 0.087 S/m for mild. We also analyzed the effect of blood perfusion in the nidus and reactive zone on the temperature reached beyond the RZ. Although tissue perfusion is known to be a crucial parameter in determining lesion size during RFA, we did not find this parameter to have a strong effect on the temperature reached in the RZ outer layer, which could be explained by the relatively narrow range of values considered for nidus perfusion $(26-70 \times 10^{-4} \text{ s}^{-1})$.

On the other hand, we did find the effect of the electrical conductivity of nidus and reactive zone to be considerable. To account for these results, we first considered an analytical model of the distributed heat q_{RF}, which is a key factor in the temperature increase. Although the geometry considered here is too complex to allow an analytical mathematical expression of q_{RF}, it can be assumed that when a voltage constant V_e is applied, q_{RF} is somehow proportional to V_e^2, and also proportional to the electrical conductivity of the tissue (σ). It is also evident that an increase in σ implies a decrease in the measured electrical impedance (Z). In our study, we observed that the change from the minimum to maximum value of either σ_n or σ_{rz} reduced Z by about 50% (see Table 2 and 3).

We can also assume that in order to keep the electrode tip temperature constant, a variation in Z will imply a variation in V_e. The power required to keep the temperature on target is V_e^2/Z. Hence, a decrease in Z (due to increased σ) should imply a drop in V_e in order to balance the required power (see Figure 6). Unlike the relation between σ and Z (which is more or less constant at 50%), the relation between Z and V_e depends on the tissue type, as can be seen in Figure 6. While an increase in σ_{rz} drastically reduces V_e (see Figure 6a), the change in V_e is minor when σ_n is changed (see Figure 6b). This could explain the distribution of q_{RF} in the reactive zone (see Figure 5), since an increase in σ_{rz} considerably reduces the applied voltage, which implies that $V_e^2 \times \sigma_{rz}$ will be globally reduced in the reactive zone, as shown in Figure 5a. On the other hand, an increase in σ_n does not seriously reduce V_e (see Figure 6a), and consequently the product $V_e^2 \times \sigma_{rz}$ will probably be more affected by σ_{rz} than V_e, i.e. the increase in σ_{rz} could be mainly responsible for the increase in q_{RF} in the reactive zone shown in Figure 5b. This could be the explanation for the higher temperature in the reactive zone when σ_{rz} is raised (see Figure 4b). Additionally, the temperature increase in the reactive zone also induces higher σ_{rz}, which further contributes to increasing q_{RF}.

In any case, this explanation is based on the simplification that q_{RF} in each tissue is proportional to $V_e^2 \times \sigma_{rz}$, V_e being the total applied voltage. The real situation of the model is probably more complex in terms of geometry (note that the electrode has a cylindrical central part but a sharp distal part) and the phenomena involved (thermal conduction has been ignored in this theoretical explanation).

The effect of RZ thickness was also analyzed. As expected, the results suggest that the thicker the reactive zone, the lower the temperature outside it. In the limiting case of RZ absent, the temperature at the outer limit of the nidus reaches 68ºC, as opposed to 44ºC at the outer limit of a 7.5 mm thick RZ. Surprisingly, increasing RZ thickness

involved a slight increase in the temperature profiles. This could be explained in the same way as the changes in σ_{rz}, i.e. since the increased thickness implies an increase in Z (see Table 2), this could bring about much higher V_e (similar to what happened when reducing σ_{rz}, see Figure 6a), and consequently an increase in q_{RF} in the reactive zone, which would be responsible for the higher temperature observed predominantly in this zone (see Figure 9).

In short, the computer results confirm that the presence of a reactive zone minimizes the thermal lesion contour in tissues beyond the reactive zone. This is reasonable: the key is to take away the point that must not be thermally damaged. However, what is surprising is the temperature increase at the boundary of the reactive zone, when this zone is less electrically conductive, as the opposite effect could be expected, i.e. more protective effect in a less conductive zone. Besides the possible explanation for this performance given above, we also believe it could be due to the fact that σ_{rz} is much smaller than σ_n. However, we conducted additional computer simulations with similar values for σ_{rz} and σ_n, and the results confirmed the general performance described: in an arrangement with two tissues (internal and external), temperature increases when electrical conductivity of the external tissue is reduced and decreases when electrical conductivity of the internal tissue is reduced.

Although the computer results can be explained thus, we should not forget the physical significance of having reactive zones with different σ_{rz} values. If a RZ such as that defined in the theoretical model has a high σ_{rz} value, it probably means that its properties are similar to those of trabecular bone, and is therefore a less reactive zone and could possibly be considered as trabecular bone. This could have the following clinical implication: although our results suggest that an increase in σ_{rz} implies a decrease in the temperature in the outer reactive zone, i.e. a protective effect, the truth is

that the area with a high σ_{rz} value represents a zone with a low degree of osteosclerosis and hence should be more thermally protected than another zone with a low σ_{rz} value.

The number of experimental studies reporting lesion sizes after RFA of OO that we could find was very limited. Furthermore, there are no experimental studies on the effect of the reactive zone characteristics on the thermal lesion. In spite of this, the computed lesion diameters in this study (1.8-2.4 cm) were in agreement with the value of 1.85 cm reported in [9] for an electrode and ablation protocol similar to our model.

We believe this to be the first computer modeling on RFA in OO. Its main limitation is probably the lack of an accurate experimental validation. Unfortunately, no previous data on temperature mapping around the OO during RFA are available for validation purpose. It also seems somewhat complex to carry out experiments in which the thickness and electrical conductivity of the reactive zone are kept under control. We suggest that future studies could use image techniques to accurately assess the geometry of the reactive zone, and even to try to infer its characteristics from the degree of osteosclerosis derived from the images.

Conclusions

The computer results suggest that the reactive zone plays the role of insulator in terms of reducing the temperature beyond it. However, they also showed an unexpected relationship between the electrical conductivity of the reactive zone, which could be related to its degree of osteosclerosis, and the ability to thermally protect the tissues beyond.

References

1. Allen SD, Saifuddin A. Imaging of intra-articular osteoid osteoma. Clin Radiol. 2003; 58; 11: 845-852.

2. Al-Omari MH, Ata KJ, Al-Muqbel KM, Mohaidat ZM, Haddad WH, Rousan LA. Radiofrequency ablation of osteoid osteoma using tissue impedance as a parameter of osteonecrosis. J Med Imaging Radiat Oncol 2012; 56: 384-389.

3. Scott SJ, Salgaonkar V, Prakash P, Burdette EC, Diederich CJ. Interstitial ultrasound ablation of vertebral and paraspinal tumours: Parametric and patient-specific simulations. Int J Hyperthermia 2014; 30: 228-244.

4. Martel J, Bueno A, Nieto-Morales ML, Ortiz EJ. Osteoid osteoma of the spine: CT-guided monopolar radiofrequency ablation. Eur J Radiol 2009; 71: 564-569.

5. Rimondi E, Mavrogenis AF, Rossi G, Ciminari R, Malaguti C, Tranfaglia C et al. Radiofrequency ablation for non-spinal osteoid osteomas in 557 patients. Eur Radiol 2012; 22: 181-188.

6. Rosenthal D, Callstrom MR. Critical review and state of the art in interventional oncology: benign and metastatic disease involving bone. Radiology 2012; 262: 765-780.

7. Bitsch RG, Rupp R, Bernd L, Ludwig K. Osteoid osteoma in an ex vivo animal model: temperature changes in surrounding soft tissue during CT-guided radiofrequency ablation. Radiology 2006; 238: 107-12.

8. Dupuy SN, Hong DE, Oliver R, Goldberg B. Radiofrequency ablation of spinal tumors: Temperature distribution in the spinal canal. AJR Am J Roentgenol 2000; 175: 1263-6.

9. Martel J, Bueno A, Domínguez MP, Llorens P, Quirós J, Delgado C. Percutaneous radiofrequency ablation: relationship between different probe types and procedure time on length and extent of osteonecrosis in dog long bones. Skeletal Radiol 2008; 37: 147-152.

10. Irastorza R M, Trujillo M, Martel Villagrán J, Berjano E. Radiofrequency ablation of osteoma osteoide: A finite element study. A. Braidot and A. Hadad (eds.), IFMBE Proceedings 49, 2015; 858-862.

11. Hall SK, Ooi EH, Payne SJ. Cell death, perfusion and electrical parameters are critical in models of hepatic radiofrequency ablation. Int J Hyperthermia. 2015;31(5):538-50.

12. Cantwell CP, O'Byrne J, Eustace S. Radiofrequency ablation of osteoid osteoma with cooled probes and impedance-control energy delivery. AJR Am J Roentgenol 2006; 186: 244-8.

13. Rana RS, Wu JS, Eisenberg RL. Periosteal reaction. AJR Am J Roentgenol 2009; 193; 4; 259-72.

14. Abraham JP, Sparrow EM. A thermal-ablation bioheat model including liquid-to-vapor phase change, pressure-and necrosis-dependent perfusion, and moisture-dependent properties. Int J Heat Mass Transfer 2007; 50; 2537-2544.

15. Schutt DJ, Haemmerich D. Effects of variation in perfusion rates and of perfusion models in computational models of radio frequency tumor ablation. Med Phys. 2008; 35:3462-70

16. Doss J D. Calculation of electric fields in conductive media, Med Phys 1982; 9: 566-573

17. Hadjipavlou P, Tzermiadianos AG, Kakavelakis MN, Lander KN. Percutaneous core excision and radiofrequency thermo-coagulation for the ablation of osteoid osteoma of the spine. Eur Spine J 2009; 18: 345-51.

18. Lindner K, Ozaki NJ, Roedl T, Gosheger R, Winkelmann G, Wörtler W. Percutaneous radiofrequency ablation in osteoid osteoma. J Bone Joint Surg Br 2001; 83: 391-96.

19. Pinto WR, Taminiau CH, Vanderschueren AHM, Hogendoorn GM, Bloem PCW, Obermann JL. Perspective: Technical considerations in CT-guided radiofrequency thermal ablation of osteoid osteoma: Tricks of the trade. AJR Am J Roentgenol 2002; 179: 1633-42.

20. Rybak LD, Gangi A, Buy X, La Rocca Vieira R, Wittig J. Thermal Ablation of Spinal Osteoid Osteomas Close to Neural Elements: Technical Considerations. AJR Am J Roentgenol 2010; 195: 293-98.

21. Haemmerich D, Webster JG. Automatic control of finite element models for temperature-controlled radiofrequency ablation. Biomed Eng Online 2005; 4; 42.

22. Hasgall PA, Di Gennaro F, Baumgartner C, Neufeld E, Gosselin MC, Payne D et al. "IT'IS Database for thermal and electromagnetic parameters of biological tissues," Version 2.6, January 13th, 2015. www.itis.ethz.ch/database

23. Tungjitkusolmun S, Staelin T, Haemmerich D, Tsai JZ, Cao H, Webster JG et al. Three-dimensional finite-element analyses for radio-frequency hepatic tumor ablation. IEEE Trans Biomed Eng 2002; 49;1: 3-9.

24. Haemmerich D, Wood BJ. Hepatic radiofrequency ablation at low frequencies preferentially heats tumour tissue. Int J Hyperthermia 2006; 22: 563-574.

25. Pätz T, Kröger T, Preusser T. Simulation of radiofrequency ablation including water evaporation. IFMBE Proceedings 2009; 25/IV:1287–90.

26. Rossmanna C, Haemmerich D. Review of temperature dependence of thermal properties, dielectric properties, and perfusion of biological tissues at hyperthermic and ablation temperatures. Crit Rev Biomed Eng 2014; 42: 6.

27. Valvano JW, Cochran JR, Diller KR. Thermal conductivity and diffusivity of biomaterials measured with self-heated thermistors. Int J Thermophys 1985; 6: 301-11.

28. Surowiec AJ, Stuchly SS, Barr JR, Swarup A. Dielectric properties of breast carcinoma and the surrounding tissues. IEEE Trans Biomed Eng 1988; 35: 257-263.

29. Klein MJ, Parisien MV, Schneider-Stock R. Osteoid osteoma. In "Pathology and Genetics of Tumours of Soft Tissue and Bone", World Health Organization Classification of Tumours, IARCPress, Lyon 2002; 260-261.

30. Mcintosh RL, Anderson V. A comprehensive tissue properties database provided for the thermal assessment of a human at rest. Biophys Rev Lett 2010; 5: 129-151.

31. Song CW, Choi IB, Nah BS, Sahu SK, Osborn JL. Microvasculature and perfusion in normal tissues and tumors. Thermoradiotherapy and Thermochemotherapy, Medical Radiology, Springer Berlin Heidelberg DA, 1995; pp. 139-156.

32. Sierpowska J, Hakulinen MA, Day JS, Weinans H, Jurvelin JS, Lappalainen R. Prediction of mechanical properties of human trabecular bone by electrical measurements. Physiol Meas 2005; 26; 2: S119.

33. Motamedi D, Learch TJ, Ishimitsu DN, Motamedi K, Katz MD, Brien EW, Menendez L. Thermal ablation of osteoid osteoma: overview and step-by-step guide. Radiographics 2009; 29; 7:2127-41.